

Mechanical Purcell filters for microwave quantum machines

Cite as: Appl. Phys. Lett. **115**, 263504 (2019); doi: [10.1063/1.5111151](https://doi.org/10.1063/1.5111151)

Submitted: 24 May 2019 · Accepted: 18 November 2019 ·

Published Online: 30 December 2019








View Online



Export Citation



CrossMark

Agnetta Y. Cleland,  Marek Pechal, Pieter-Jan C. Stas,  Christopher J. Sarabalis,  E. Alex Wollack, 
and Amir H. Safavi-Naeini^{a)} 

AFFILIATIONS

Department of Applied Physics and Ginzton Laboratory, Stanford University, 348 Via Pueblo Mall, Stanford, California 94305, USA

^{a)}Electronic mail: safavi@stanford.edu

ABSTRACT

In circuit quantum electrodynamics, measuring the state of a superconducting qubit introduces a loss channel, which can enhance spontaneous emission through the Purcell effect, thus decreasing the qubit lifetime. This decay can be mitigated by performing the measurement through a Purcell filter, which strongly suppresses signal propagation at the qubit transition frequency. If the filter is also well-matched at the readout cavity frequency, it will protect the qubit from decoherence channels without sacrificing measurement bandwidth. We propose and analyze design for a mechanical Purcell filter, which we also fabricate and characterize at room temperature. The filter is composed of an array of nanomechanical resonators in thin-film lithium niobate, connected in a ladder topology, with series and parallel resonances arranged to produce a bandpass response. Their modest footprint, steep band edges, and lack of cross talk make these filters an appealing alternative to analogous electromagnetic versions currently used in microwave quantum machines.

Published under license by AIP Publishing. <https://doi.org/10.1063/1.5111151>

Quantum information processing calls for systems that are well isolated from their environment, whose states can nonetheless be measured and manipulated with precision.¹ These fundamentally contradictory requirements can be satisfied by cleverly engineering devices and interactions between them. In the circuit QED platform,^{2,3} nonlinear superconducting circuits called qubits are used to store and process quantum information. Their internal states need to be read out rapidly and with low rates of error. An appealing approach for this is to couple the qubit circuit to an auxiliary, linear electromagnetic resonator (often called the readout cavity). Resonators have long been used to amplify emission from atoms, for instance, via Purcell enhancement.^{4–6} Conversely, qubit emission into the environment can be suppressed by tuning the qubit away from the resonator's frequency by many times the qubit and resonator linewidths and their mutual interaction energy. The qubit state is then measured “dispersively” by monitoring the resonator frequency for shifts induced by changes in the qubit state³ (although we note that alternative measurement strategies exist).⁷

Dispersive shifts of the cavity can be measured and amplified to demonstrate extremely efficient single-shot measurements of qubits using this scheme.^{8–10} Nonetheless, the conflicting requirements of efficient readout and qubit isolation persist in the desired properties of

the resonator-qubit system.¹¹ Fast and efficient readout requires strong coupling between the resonator and the environment. This in turn increases the probability of qubit relaxation through the resonator in a process called Purcell decay.^{4,12–14} Purcell filters, often consisting of a second stage electromagnetic resonator, have been used effectively to mitigate this process.^{10,15–19}

As qubit coherence times continue to improve, the basic limit imposed by Purcell decay will become more important. In principle, progressively higher order electromagnetic filters can be incorporated, requiring progressively larger components that take up valuable space on a chip. We propose an alternative solution using ultracompact, high-order microwave acoustic filters to isolate qubits from the environment and to curtail Purcell decay, using techniques adapted from the telecommunication industry.^{20,21} Low cross talk and extremely small footprints make nanomechanical structures ideal for integration with superconducting quantum machines.^{22–27} In filters that occupy less than 0.25 mm² on-chip, we measure –60 dB suppression out of band, with passbands spanning up to 300 MHz at 3.9 GHz. Moreover, recent advances in fabrication and design of thin-film, high-Q, and strongly coupled lithium niobate (LN) devices make them well-suited for such applications.^{26–28} In this manuscript, we outline the approach and present initial experimental results.

The cavity-qubit interaction is described by the Jaynes–Cummings Hamiltonian,

$$\hat{H}_{\text{JC}} = \hbar\omega_r \left(\hat{a}^\dagger \hat{a} + \frac{1}{2} \right) + \frac{\hbar\omega_q}{2} \hat{\sigma}_z + \hbar g (\hat{a}^\dagger \hat{\sigma}_- + \hat{a} \hat{\sigma}_+), \quad (1)$$

where ω_r is the readout resonator frequency, g is the qubit-resonator coupling strength, \hat{a} annihilates photons in the resonator, and Pauli operators $\hat{\sigma}$ act on the qubit. This Hamiltonian can be diagonalized into a series of n -excitation subspaces, each spanned by $|g, n\rangle$ and $|e, n-1\rangle$. For $|g| \gg |\Delta|$, the “qubitlike” polariton in the first excited subspace is

$$|+, 1\rangle \approx |e, 0\rangle + \frac{g}{\Delta} |g, 1\rangle.$$

The small but finite occupation of the resonator represented by $|g, 1\rangle$ can decay to $|g, 0\rangle$ through the resonator’s output channel, effectively causing the atom to relax to its ground state. This loss channel increases the decay rate of the qubit by $\gamma_q = \kappa | \langle g, 0 | \hat{a} | +, 1 \rangle |^2 \approx g^2 \kappa / \Delta^2$. More generally, we can use Fermi’s golden rule to calculate the decay of the qubit excited state $|e, n\rangle$ through the resonator,

$$\gamma_q = \frac{g^2 \kappa}{\Delta^2 + (\kappa/2)^2} \xrightarrow{\Delta \gg \kappa, g} \frac{g^2}{\Delta^2} \kappa. \quad (2)$$

This allows us to choose Δ such that the maximum coherence time imposed by the Purcell effect $1/\gamma_q$ exceeds the qubit’s T_1 due to other sources. With improving qubit design, fabrication, and materials processing, larger detunings Δ will be required to avoid limitation by Purcell decay. However, since g cannot be increased indefinitely due to geometric constraints, increasing Δ reduces the state-dependent cavity shift $\chi \approx g^2/\Delta$. This further complicates readout optimization: the ratio $\chi/\kappa = 1/2$ gives optimal pointer state discrimination, and large κ is desirable for quick extraction of information from the cavity.^{10,29} Reducing χ increases the amount of time required to make a measurement, which can allow for more errors to be introduced. These inconveniences have led to the design and implementation of Purcell filters. These filters, previously composed of electromagnetic resonators, protect the qubit from the Purcell decay channel while maintaining the ability to perform fast and accurate measurements of the qubit state.

A Purcell filter can be considered to be, in one possible implementation, a bandpass filter that performs an impedance transformation on the dissipative bath of the environment, through which the linear resonator can be probed. Placing the qubit frequency outside the passband where the filter presents an impedance mismatch isolates the qubit from energy relaxation channels of the vacuum; placing the resonator frequency within the passband allows a microwave tone to pass through unimpeded and probe the resonator frequency. The resonator can be strongly coupled to its feed line (large κ), allowing signals to pass through the cavity quickly for fast qubit state measurement, without risking a reduction in qubit lifetime.

In design and analysis, we treat the mechanical filter as a two port microwave system connected at one end to a regular transmission line and at the other end to the readout resonator (Fig. 1). The impedance $Z_{\text{ext}}(\omega)$ seen by the resonator captures all properties of the filter element relevant to qubit operation. In this section, we develop an understanding of how $Z_{\text{ext}}(\omega)$ affects qubit readout and Purcell decay.

A relevant figure of merit for a Purcell filter is the ratio of qubit lifetimes with and without the filter in place. In this ratio, the capacitance

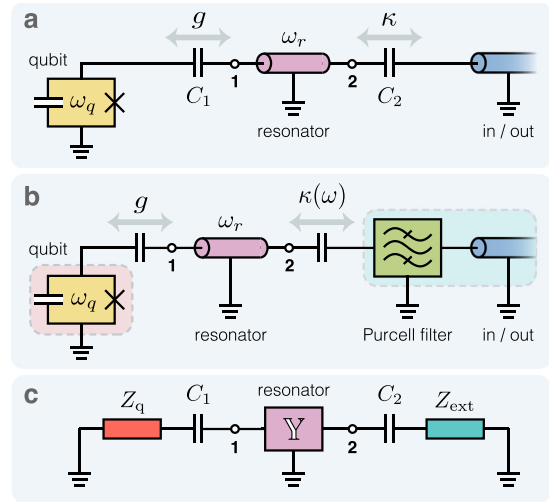


FIG. 1. Dispersive qubit readout. (a) Conventional schematic for measuring the energy state of a superconducting qubit (orange) with a transition frequency ω_q . The qubit is coupled at a rate g to a linear resonator (pink) with a fundamental resonance at ω_r and a leakage rate κ to its input and output transmission line (blue). The coupling rates g and κ are controlled by the capacitances C_1 and C_2 . (b) By driving the auxiliary resonator through the passband of a Purcell filter (green), one can modify the external dissipation presented to the resonator and qubit, so that now κ and consequently T_1 include a frequency dependence. (c) To derive the filter’s effect on the qubit lifetime, we replace the filter and environmental dissipation with their equivalent impedance Z_{ext} and the qubit with its impedance Z_q . The resonator response is encapsulated by its admittance matrix \mathbb{Y} , taken with respect to nodes 1 and 2.

C_2 is adjusted to keep the resonator linewidth fixed. We can derive this ratio using a method complementary to those of Refs. 16 and 17 by analyzing the measurement circuitry depicted in Fig. 1(c), in which the capacitances C_1 and C_2 are assumed to be small. The admittance matrix for the entire system, with respect to nodes 1 and 2, is given by

$$\mathbb{Y} + \begin{bmatrix} 1 & 0 \\ 1/i\omega C_1 + Z_q & 1 \\ 0 & 1 \\ & 1/i\omega C_2 + Z_{\text{ext}} \end{bmatrix} \approx \mathbb{Y} + \begin{bmatrix} \omega^2 C_1^2 Z_q & 0 \\ 0 & \omega^2 C_1^2 Z_{\text{ext}} \end{bmatrix},$$

where we absorb the reactive part of the admittance matrix with \mathbb{Y} into $\bar{\mathbb{Y}}$. We solve for the resonances by setting the determinant of the above expression to 0. These solutions are small deviations from the uncoupled case: the resonator mode shifts to $\omega_r + \delta\omega_r$ and the qubit frequency that satisfies $Z_q(\omega_q) \rightarrow \infty$ shifts to $\omega_q + \delta\omega_q$. Keeping lowest-order terms in the small capacitances, we find

$$\delta\omega_r = + \frac{\omega_r^2 C_1^2 \bar{\mathbb{Y}}_{22}(\omega_r)}{Y'_q(\omega_q) \Delta \lambda} - \frac{\omega_r^2 C_2^2 Z_{\text{ext}}(\omega_r) \bar{\mathbb{Y}}_{11}(\omega_r)}{\lambda},$$

$$\delta\omega_q = - \frac{\omega_q^2 C_1^2 \bar{\mathbb{Y}}_{22}(\omega_q)}{Y'_q(\omega_q) \Delta \lambda} + \frac{\omega_q^4 C_1^2 C_2^2 Z_{\text{ext}}(\omega_q) \bar{\mathbb{Y}}_{22}(\omega_q) \bar{\mathbb{Y}}_{11}(\omega_q)}{Y'_q(\omega_q) \Delta^2 \lambda^2},$$

where $\lambda = \frac{d}{d\omega} \det \bar{\mathbb{Y}}(\omega)|_{\omega=\omega_r}$, $Y_q(\omega) = 1/Z_q(\omega)$, and $Y' = dY/d\omega$. The coupling strength g can be found by equating the first term in the

cavity shift to g^2/Δ and approximating $|\Delta| \ll \omega_{q,r}$ to find $-g^2 \approx \omega_r^2 C_1^2 \nabla_{22}(\omega_r)/Y'_q(\omega_q)\lambda$. The frequency shift $\chi \approx g^2/\Delta$ arises from the qubit-resonator coupling and forms the basis of dispersive qubit readout.^{11,30,31} External dissipation Z_{ext} introduces a small imaginary component to the frequency shifts, from which we extract the resulting qubit and resonator linewidths $\gamma_q, \kappa = 2 \text{Im} \delta\omega_{q,r}$ to find

$$\gamma_q = \frac{g^2 \text{Re} Z_{\text{ext}}(\omega_q)}{\Delta^2 \text{Re} Z_{\text{ext}}(\omega_r)} \kappa. \quad (3)$$

Without a filter, when $Z_{\text{ext}}(\omega_r) = Z_{\text{ext}}(\omega_q) = Z_0$, this reduces to the familiar Purcell decay rate of Eq. (2). The filter adds an extra degree of protection from spontaneous emission, a “filter factor,” which is the ratio of the resistances seen by the qubit and resonator at their respective frequencies.

The mechanical Purcell filter is based on a ladder network of piezoelectric oscillators, inspired by methods that are ubiquitous in classical RF and telecommunication technology.^{20,21} A ladder filter electrically connects series and shunt resonators with frequencies carefully chosen to produce a bandpass response [Figs. 2 and 4(a)]. The series resonators are identical to each other, as are the shunt (parallel) resonators.

Each resonator’s electrical response is described by its admittance $Y(\omega) = 1/Z(\omega)$, where $Z(\omega)$ is the electrical impedance. This response is well-modeled by a Modified Butterworth-van Dyke (MBVD) equivalent circuit (Fig. 2).^{20,32} It is important that the antiresonance of the parallel resonators—the zero in $Y_p(\omega)$ —is placed at the series resonance or the pole in $Y_s(\omega)$ [Fig. 4(a)]. This frequency defines the center of the passband: here, the parallel resonators have maximal impedance, while the series resonators have minimal impedance, so a microwave signal passes easily through the filter. The spacing between each resonance f_R and its antiresonance f_A is given by the electromechanical coupling factor $k^2 = (\pi^2/8)(f_A^2 - f_R^2)/f_A^2$.³² This

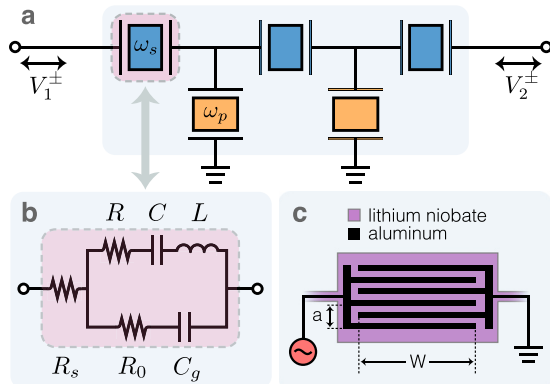


FIG. 2. Nanomechanical ladder filter design. (a) Ladder topology of order 3 in which each colored block represents an acoustic element. Three identical series resonators (blue) at ω_s are shunted by two identical parallel resonators (orange) at $\omega_p \neq \omega_s$. The highlighted element is detailed in (b) for its electrical response and (c) for its basic physical design. (b) Modified Butterworth-van Dyke equivalent circuit that models a single mechanical resonator. The transducer’s electrostatic capacitance C_g is connected in parallel with a series RLC that parameterizes the acoustic resonance. R_s and R_0 model resistive loss in the electrodes and dielectric loss, respectively. (c) Diagram of a single resonator. A suspended plate of lithium niobate is patterned with aluminum interdigitated transducers of pitch a and width W .

spacing relates the spectral distance between the filter edges and its center [Fig. 4(a)]. Thus, it can be seen that k^2 , which depends strongly on the material platform, determines the filter bandwidth. The MBVD circuit fully parameterizes the frequency ($\omega_m = 1/\sqrt{LC}$), piezoelectric coupling ($k^2 = \pi^2 C/8C_g$), and quality factor ($Q = \pi^2/8 \omega_m CR$) of each mechanical resonance.³²

While the quality factor of the resonators contributes to insertion loss in the passband and less sharply defined band edges, it is not a strong limiting factor in filter performance [Fig. 4(b)]. This is because the measurement occurs in the qubit-cavity interaction with little participation of the mechanical elements. We plot a filter’s enhancement of qubit relaxation time in Fig. 4(c). Notably, T_1 is sensitive to R_0 and R_s . A well-matched filter has $\text{Re} Z_{\text{ext}}(\omega_r) \approx Z_0$, and so according to Eq. (3), the suppression of γ_q is limited by $\text{Re} Z_{\text{ext}}(\omega_q)/Z_0$. Finally, we note that the electromechanical coupling factor^{33,34}—an indicator of the conversion efficiency between electrical and mechanical energies—can be varied by rotating the interdigitated transducers (IDTs) relative to the crystal axes [Fig. 5(a)] to select different components of the piezoelectric tensor. It can also be increased by patterning IDTs with larger N .

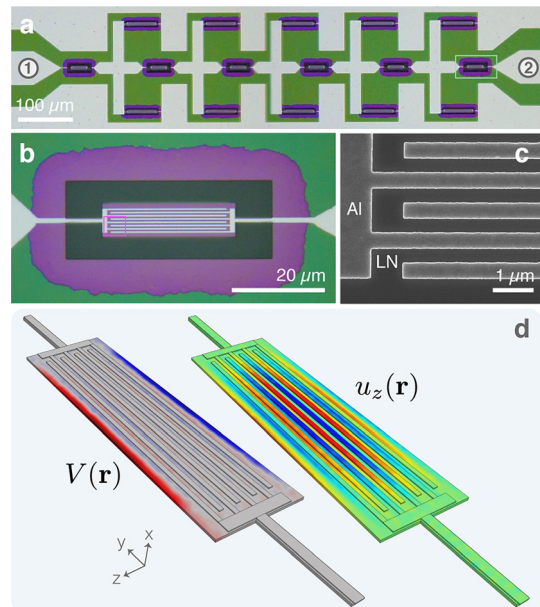


FIG. 3. Device layout. (a) Real-color optical micrograph of the 10° filter analyzed in Fig. 5(a). Where the LN film has been released from the silicon substrate, it appears purple, while unreleased regions appear green. Etched gaps in the LN film appear black. Aluminum electrodes and surrounding ground plane (gray) are contacted by a three-point (ground-signal-ground) coplanar waveguide probe. The ground planes above and below the filter are connected around each contact pad (not pictured). Transmission measurements in Fig. 5 are made with respect to the indicated ports 1 and 2. (b) Optical micrograph detailing the sixth series resonator, highlighted in (a). This resonator has a pitch of $a = 1.487 \mu\text{m}$, a width of $W = 25 \mu\text{m}$, and $N = 4$ IDT pairs. (c) Scanning electron micrograph detailing the electrode geometry of (b). (d) Finite-element simulation of a longitudinal Lamb mode at $\omega_m = 2\pi \times 3.74 \text{ GHz}$. The z -component of displacement $u_z(\mathbf{r})$ and corresponding electrostatic potential $V(\mathbf{r})$ are plotted. The coordinate system corresponds to the LN crystal axes.

We fabricate our devices on X-cut LN using a process similar to that described in Ref. 26. The IDTs are defined by electron beam lithography in a 100 nm aluminum film, deposited on top of 250 nm of LN, which is first patterned and etched by argon ion milling. The LN devices are released from the substrate by removing the underlying silicon in an isotropic xenon difluoride vapor etch. A fully fabricated device is shown in Fig. 3. Each series resonator (middle row) is shunted by two parallel resonators with total admittance Y_p . This geometry is chosen to symmetrize electromagnetic fields above and below the signal line, to avoid creating parasitic microwave modes.³⁵

We measure the scattering parameters of fabricated filters using a calibrated vector network analyzer at room temperature and atmospheric pressure. The calibration is done using short, open, and matched loads and through connections on a calibration substrate purchased from GGB Industries, which shifts the reference plane of the measurement to the probe tips. Reflection and transmission are

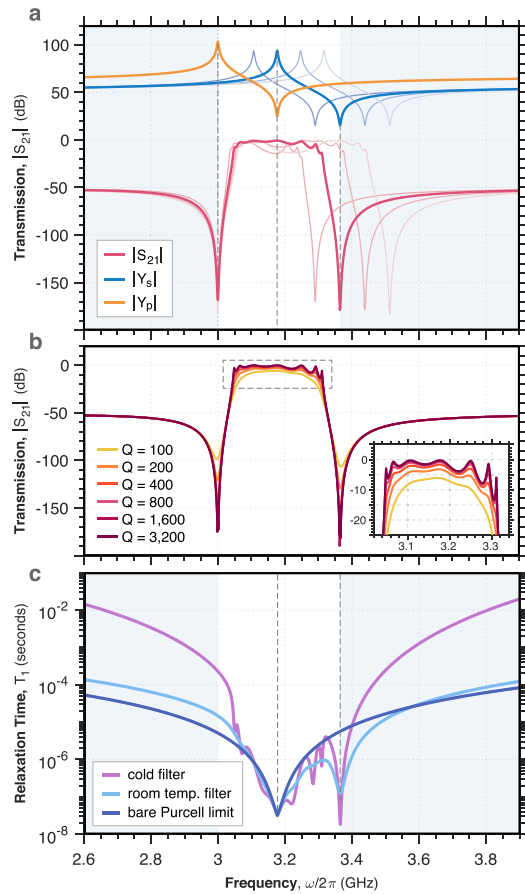


FIG. 4. Circuit analysis. (a) Filter response for different detunings of the series resonance, computed by the MBVD model. (b) Filter response for $\omega_p = 2\pi \times 3.00$ GHz and $\omega_s = 2\pi \times 3.18$ GHz for different values of $Q_s = Q_p = Q$ with $R_s = R_0 = 0$. (c) Projected enhancement of qubit T_1 with the addition of a Purcell filter, with the readout resonator frequency centered in the passband at $\omega_r = \omega_s = 2\pi \times 3.18$ GHz. This enhancement is calculated according to Eqs. (3) and (4) for the geometry corresponding to the bold traces in (a), which have $Q = 800$. We set $R_s = R_0 = 10 \Omega$ to model room temperature behavior and $R_s = R_0 = 0$ to model cryogenic temperatures.

analyzed to calculate the filter enhancement factor on the qubit lifetime described by Eq. (3). The impedance mismatch limits the transmission in the passband to below -10 dB in the first four devices. We can increase the capacitance to improve matching to the filter by replacing each series and parallel element with a stack of identical parallelized resonators. The 60° P device in Fig. 5 replaces each series element with $n_s = 6$ parallelized resonators and $n_p = 3$ for each parallel element (see the supplementary material). The environmental impedance can be extracted from calibrated measurements of a filter's scattering parameters by³⁶

$$\text{Re } Z_{\text{ext}} = Z_0 \frac{1 - |S_{11}|^2}{|1 - S_{11}|^2}. \quad (4)$$

We calculate unfiltered Purcell-limited and filter-enhanced T_1 for a qubit-resonator system with constant g and κ , shown in Fig. 5. The bare Purcell rate is found by diagonalizing Eq. (1), using a single-mode resonator model, without assuming $g \ll \Delta$ in the mixing angle $\tan 2\theta_n = 2g\sqrt{n}/\Delta$.^{30,31} We see from Fig. 5(b) that the filter realizes nearly one order of magnitude of improvement in qubit T_1 over the

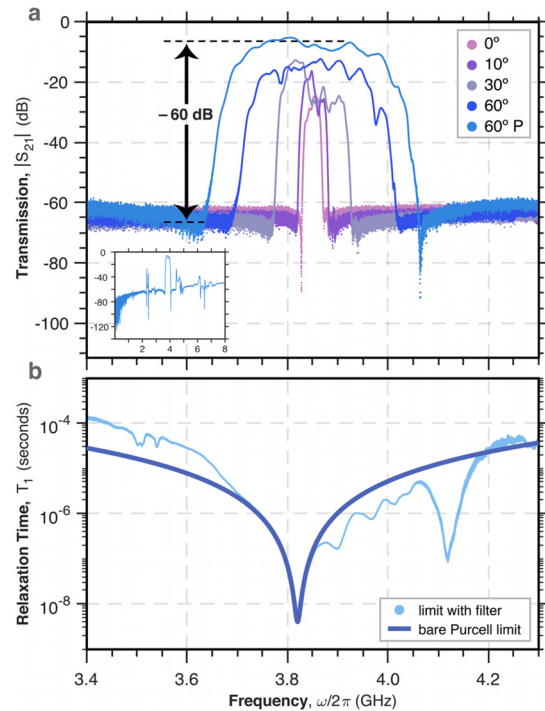


FIG. 5. Filter characterization. (a) Room temperature transmission spectra. Each device is rotated (as indicated) counterclockwise to produce an angle θ between the mechanical propagation direction and the LN extraordinary axis, and P indicates a device with parallelized series and shunt elements. The center frequencies are shifted by ± 200 MHz to align the passbands for ease of viewing. The x-axis labels correspond to the 60° P device. The inset shows $|S_{21}|$ of this device up to 8 GHz. (b) Calculated raw Purcell-limited and filter-enhanced energy relaxation times T_1 as a function of qubit frequency. This model centers the resonator frequency $\omega_r = 2\pi \times 3.82$ GHz in the filter passband and assumes constant coupling to the qubit $g = 2\pi \times 10$ MHz and resonator leakage rate $\kappa = 2\pi \times 10$ MHz. Filtered T_1 is calculated from Eqs. (3) and (4) using S_{11} measurements from the 60° P device shown in (a).

TABLE I. Designed device parameters for measurements in Fig. 5: pitch a , number of IDT pairs N , and width W are reported for series (subscript s) and parallel (subscript p) components of each device. The last row describes both the 60° and 60° P devices.

a_s (μm)	N_s	W_s (μm)	a_p (μm)	N_p	W_p (μm)	θ ($^\circ$)	Order
1.489	4	15	1.500	4	50	0	6
1.487	4	25	1.500	4	50	10	6
1.466	4	25	1.500	4	50	30	6
1.365	4	25	1.500	6	50	60	6

unfiltered system. We expect greater enhancement at cryogenic temperatures, where $R_s, R_0 \rightarrow 0$ as shown in Fig. 4(c). Design parameters for the filter measurements shown in Fig. 5 are reported in Table I.

We have proposed and realized Purcell filters that use nanomechanical elements in a qubit-compatible platform.^{26,27} Through room temperature measurements, we quantify the expected enhancement of the relaxation time for a range of qubit frequencies around the passband. While our devices operate at 3.5–4 GHz, higher frequencies can be achieved by patterning IDTs with a smaller pitch. We have fabricated resonators of this style in the 6–7 GHz range without difficulty. We show that the bandwidths of these filters can be tuned by design, reaching up to 300 MHz, which is broad enough to accommodate many strongly coupled resonators for fast, multiplexed qubit readout. Quantum acoustic systems have been proposed as a means of realizing memory elements for processors^{25,37} and quantum state converters for networking.^{38–40} Our work opens a space in the field for acoustic systems that can impact the development of quantum machines.

See the [supplementary material](#) for further characterization of mechanical resonators and filter parallelization.

The authors thank P. Arrangoiz-Arriola, T. P. McKenna, and W. Jiang for useful discussions. This work was supported by the U.S. government through the Department of Energy Grant No. DE-SC0019174 and the National Science Foundation Grant Nos. ECCS-1808100 and PHY-1820938. A.Y.C. was supported by a Stanford Graduate Fellowship. Part of this work was performed at the Stanford Nano-Shared Facilities (SNSF), supported by the National Science Foundation under Grant No. ECCS-1542152, and the Stanford Nanofabrication Facility (SNF).

REFERENCES

- D. P. DiVincenzo, *Fortschr. Phys.* **48**, 771 (2000).
- M. H. Devoret and R. J. Schoelkopf, *Science* **339**, 1169 (2013).
- J. Koch, T. M. Yu, J. Gambetta, A. A. Houck, D. I. Schuster, J. Majer, A. Blais, M. H. Devoret, S. M. Girvin, and R. J. Schoelkopf, *Phys. Rev. A* **76**, 042319 (2007).
- E. M. Purcell, *Phys. Rev.* **69**, 37 (1946).
- P. Goy, J. M. Haimond, M. Gross, and S. Haroche, *Phys. Rev. Lett.* **50**, 1903 (1983).
- S. M. Girvin, “Circuit QED: Superconducting qubits coupled to microwave photons,” in *Quantum Machines: Measurement and Control of Engineered Quantum Systems*, edited by M. Devoret, B. Huard, R. Schoelkopf, and L. Cugliandolo (Oxford University Press, 2014).
- N. Didier, J. Bourassa, and A. Blais, *Phys. Rev. Lett.* **115**, 203601 (2015).
- R. Vijay, D. H. Slichter, and I. Siddiqi, *Phys. Rev. Lett.* **106**, 110502 (2011).
- E. Johnson, C. Macklin, D. H. Slichter, R. Vijay, E. B. Weingarten, J. Clarke, and I. Siddiqi, *Phys. Rev. Lett.* **109**, 050506 (2012).
- T. Walter, P. Kurpiers, S. Gasparinetti, P. Magnard, A. Potocnik, Y. Salathé, M. Pechal, M. Mondal, M. Oppliger, C. Eichler, and A. Wallraff, *Phys. Rev. Appl.* **7**, 054020 (2017).
- P. Krantz, M. Kjaergaard, F. Yan, T. P. Orlando, S. Gustavsson, and W. D. Oliver, *Appl. Phys. Rev.* **6**, 021318 (2019).
- A. A. Houck, D. I. Schuster, J. M. Gambetta, J. A. Schreier, B. R. Johnson, J. M. Chow, L. Frunzio, J. Majer, M. H. Devoret, S. M. Girvin, and R. J. Schoelkopf, *Nature* **449**, 328 (2007).
- J. M. Gambetta, A. A. Houck, and A. Blais, *Phys. Rev. Lett.* **106**, 030502 (2011).
- A. A. Houck, J. A. Schrier, B. R. Johnson, J. M. Chow, J. Koch, J. M. Gambetta, D. I. Schuster, L. Frunzio, M. H. Devoret, S. M. Girvin, and R. J. Schoelkopf, *Phys. Rev. Lett.* **101**, 080502 (2008).
- M. D. Reed, B. R. Johnson, A. A. Houck, L. DiCarlo, J. M. Chow, D. I. Schuster, L. Frunzio, and R. J. Schoelkopf, *Appl. Phys. Lett.* **96**, 203110 (2010).
- E. Jeffrey, D. Sank, J. Y. Mutus, T. C. White, J. Kelly, R. Barends, Y. Chen, Z. Chen, B. Chiaro, A. Dunsforth, A. Megrant, P. J. J. O’Malley, C. Neill, P. Roushan, A. Vainsencher, J. Wenner, A. N. Cleland, and J. M. Martinis, *Phys. Rev. Lett.* **112**, 190504 (2014).
- E. A. Sete, J. M. Martinis, and A. N. Korotkov, *Phys. Rev. A* **92**, 012325 (2015).
- N. T. Bronn, Y. Liu, J. B. Hertzberg, A. D. Córcoles, A. A. Houck, J. M. Gambetta, and J. M. Chow, *Appl. Phys. Lett.* **107**, 172601 (2015).
- J. Heinsoo, C. K. Andersen, A. Remm, S. Krinner, T. Walter, Y. Salathé, S. Gasparinetti, J.-C. Besse, A. Potocnik, A. Wallraff, and C. Eichler, *Phys. Rev. Appl.* **10**, 034040 (2018).
- D. Morgan, *Surface Acoustic Wave Filters* (Academic Press, 2007).
- K.-Y. Hashimoto, *RF Bulk Acoustic Wave Filters for Communications* (Artech House, 2009).
- P. Arrangoiz-Arriola and A. H. Safavi-Naeini, *Phys. Rev. A* **94**, 063864 (2016).
- K. J. Satzinger, Y. P. Zhong, H.-S. Chang, G. A. Peairs, A. Bienfait, M.-H. Chou, A. Y. Cleland, C. R. Conner, É. Dumur, J. Grebel, I. Gutierrez, B. H. November, R. G. Povey, S. J. Whiteley, D. D. Awschalom, D. I. Schuster, and A. N. Cleland, *Nature* **563**, 661 (2018).
- Y. Chu, P. Kharel, W. H. Renninger, L. D. Burkhardt, L. Frunzio, P. T. Rakich, and R. J. Schoelkopf, *Science* **358**, 199 (2017).
- M. Pechal, P. Arrangoiz-Arriola, and A. H. Safavi-Naeini, *Quantum Sci. Technol.* **4**, 015006 (2019).
- P. Arrangoiz-Arriola, E. A. Wollack, M. Pechal, J. D. Witmer, J. T. Hill, and A. H. Safavi-Naeini, *Phys. Rev. X* **8**, 031007 (2018).
- P. Arrangoiz-Arriola, E. A. Wollack, Z. Wang, M. Pechal, W. Jiang, T. P. McKenna, J. D. Witmer, and A. H. Safavi-Naeini, *Nature* **571**, 537 (2019).
- C. J. Sarabalis, Y. D. Dahmani, A. Y. Cleland, and A. H. Safavi-Naeini, preprint [arXiv:1904.04981](#) (2019).
- J. Gambetta, A. Blais, M. Boissonneault, A. A. Houck, D. I. Schuster, and S. M. Girvin, *Phys. Rev. A* **77**, 012112 (2008).
- D. I. Schuster, “Circuit quantum electrodynamics,” Ph.D. thesis (Yale University, 2007).
- M. D. Reed, “Entanglement and quantum error correction with superconducting qubits,” Ph.D. thesis (Yale University, 2013).
- F. V. Pop, A. S. Kochhar, G. Vidal-Alvarez, and G. Piazza, “Laterally vibrating lithium niobate MEMS resonators with 30% electromechanical coupling coefficient,” in Proceedings of the IEEE 30th International Conference on Micro-Electro Mechanical Systems (MEMS) (2017), p. 966.
- IEEE Standard on Piezoelectricity, *ANSI/IEEE Standard 176-1987* (IEEE, 1988).
- Q.-M. Wang, X.-H. Du, B. Xu, and L. E. Cross, *IEEE Trans. Ultrason., Ferroelectr., Freq. Control* **46**, 3 (1999).
- G. E. Ponchak, J. Papapolymerou, and M. M. Tentzeris, *IEEE Trans. Microwave Theory Tech.* **53**, 713–717 (2005).
- D. M. Pozar, *Microwave Engineering* (Wiley, 2012).
- A. N. Cleland and M. R. Geller, *Phys. Rev. Lett.* **93**, 070501 (2004).
- A. H. Safavi-Naeini and O. Painter, *New J. Phys.* **13**, 013017 (2011).
- C. A. Regal and K. W. Lehnert, *J. Phys.: Conf. Ser.* **264**, 012025 (2011).
- G. Kurizki, P. Bertet, Y. Kubo, K. Molmer, D. Petrosyan, P. Rabl, and J. Schmiedmayer, *Proc. Natl. Acad. Sci.* **112**, 3866 (2015).